Analytical Compensation for Spatially Variant Detector Response in SPECT With Varying Focal-Length Fan-Beam Collimators

Tianfang Li, *Member, IEEE,* Junhai Wen, *Member, IEEE,* and Zhengrong Liang, *Member, IEEE*

***Abstract*—The authors present a new method to compensate for the spatially variant detector response in single photon emission computed tomography (SPECT) with varying focal-length fan-beam (VFF) geometry. In this method, the deblurred projection is explicitly expressed as an integral of the collimator blurred data and the fully calibrated system kernel matrix with certain transforms. It needs a little more computation time than the conventional filtering techniques but provides much more accurate compensation. This method also represents a unified framework for detector response compensation in parallel-hole fan-beam and VFF SPECT with a circular scan orbit.**

***Index Terms*—Spatially variant detector response, SPECT, VFF collimators.**

I. Introduction

IT IS WELL known that the spatially varying focal-length fan-beam (VFF) collimation has the advantages of improving sensitivity and resolution (as compared to parallel-hole geometry) without truncation problem (as compared to fan-beam geometry) in single photon emission computed tomography (SPECT). However, there is always unavoidable detector blurring effect due to the finite size of the collimator holes in SPECT imaging. The detector response in reality is spatially varying and deteriorates with distance from the face of the collimators. It results in shape distortions and nonuniform density variations in the reconstructed images. Compensation for this degrading effect accurately and efficiently is a quite challenging task, especially for nonparallel collimators due to their relatively more complicate geometries.

To date, the most accurate approach to compensate for the nonstationary detector response is to use iterative reconstruction algorithms which incorporate an accurate model of photon transport from the body to the detector [1]–[5]. Unfortunately, these algorithms often require a regulation for adequate convergence and an intensive computing effort, which are not feasible for clinical use. A limited number of noniterative methods have been also proposed for the compensation of the nonstationary detector response which utilize the filtering techniques based on the frequency-distance relation (FDR) [6]–[12], but they do not work very well, especially in nonparallel geometries. The limitation is discussed later in this paper.

Analytical compensation for the detector blurring effect in nonparallel geometries becomes more attractive and feasible since the discovery of inversion formula for nonuniformly attenuated Radon transform by Novikov, *et al.* [13], [14], because a complete noniterative reconstruction framework could be established with simultaneous consideration of Poisson noise, Compton scatter, nonuniform attenuation, and nonstationary detector response. Research efforts have been made for parallel-beam SPECT [15]. For both fan-beam and VFF geometries, it has been shown that an analytical reconstruction method can be derived with compensation for the nonuniform attenuation [16], [17]. In this work, our efforts are focused on the compensation for the nonstationary detector response in the VFF geometry analytically (where fan-beam geometry can be treated as a special case), so that a complete noniterative reconstruction framework for VFF and fan-beam collimated SPECT can be established in a similar manner as [15].

For this purpose, we investigated the system response and the FDR [6], [7] in fan-beam and VFF geometries, and studied the limitation of the FDR-based filtering techniques for the nonparallel geometries. Based on the investigation, we then developed a new analytical method to incorporate the fully calibrated system response matrix. In this method, a new kernel matrix was derived using singular value decomposition (SVD) of the system response matrix in the frequency domain, with which the detector blurred projection data can be accurately compensated. This *kernel matrix method* provides a unified framework for compensation of detector response in parallel-hole fan-beam and VFF collimated SPECT with a circular orbit.

In the following, we first present our definitions and background knowledge of the detector response model in Section II; then, we discuss the limitation of the FDR-filtering method in fan-beam and VFF geometries and propose our new method utilizing the fully calibrated system imaging matrix in Section III. In Section IV, simulation results are presented to show the potential of the proposed method in both sinogram and reconstructed image spaces.

Manuscript received on December 2, 2002; revised March 19, 2003. This work was supported in part by the National Institute of Health National Heart, Lung and Blood Institute under Grant HL54166.

T. Li is with the Departments of Physics and Astronomy and Radiology, State University of New York, Stony Brook, NY 11790 USA (e-mail: tfli@clio.mil.sunysb.edu).

J. Wen is with the Department of Radiology, State University of New York, Stony Brook, NY 11794 USA (e-mail: wenjh@clio.mil.sunysb.edu).

Z. Liang is with the Departments of Radiology and Computer Science, State University of New York, Stony Brook, NY 11794 USA (e-mail: jzl@clio.mil.sunysb.edu).

Digital Object Identifier 10.1109/TNS.2003.812440

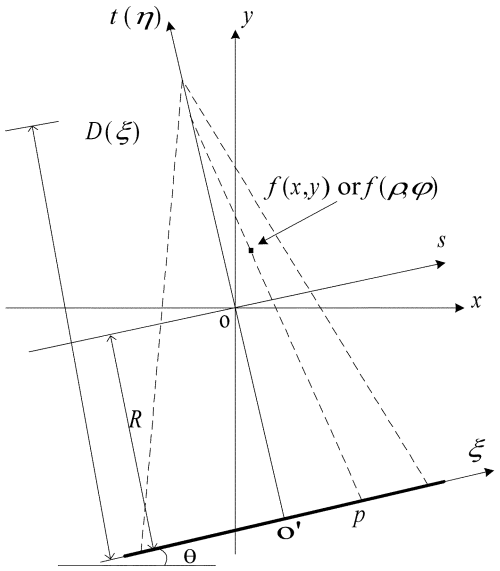

Fig. 1. CCS and other coordinate systems in VFF SPECT.

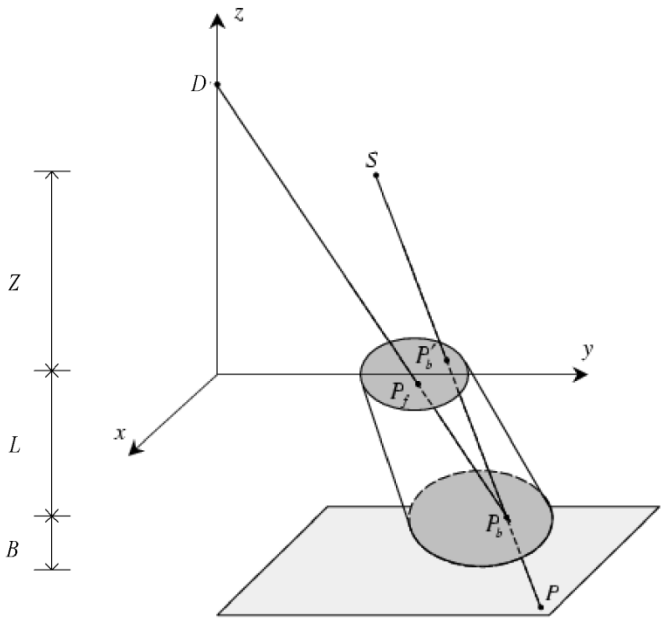

Fig. 2. Geometrical model for the point-spread function of VFF collimators. Point source is located at a distance Z from the collimator face. L is the collimator thickness, and B is the distance between the collimator backplane and the image plane inside the scintillation crystal.

II. Basic Notations and Background Review

Described below are the collimator coordinate system (CCS) and the geometric transfer function (GTF) model for the detector response, which are related to the derivation of the FDR.

A. Collimator Coordinate System and Basic Notations

To develop the GTF and FDR for any detector system, we introduce a general "collimator coordinate system" or the CCS of ξ-η as shown in Fig. 1, restricted to one slice for simplicity. The CCS is detailed as follows: any point in this coordinate system is represented by (ξ, η), where ξ is defined as the location on the detection plane where the point is being projected, and η is the distance from the point to the detection plane. More precisely, the focal point, the source point, and the detecting point lie in one straight line.

The other two coordinate systems shown in Fig. 1 are fixed system x-y and rotated coordinate system s-t. Note that the origins of ξ-η and s-t are o and o', respectively. Relationships among these coordinate systems are

$$(x, y) = (\rho\cos\varphi, \rho\sin\varphi) \tag{1}$$

$$(s, t) = (x\cos\theta + y\sin\theta, -x\sin\theta + y\cos\theta) \tag{2}$$

$$(\xi, \eta) = \left(\frac{sD(\xi)}{D(\xi) - R - t}, R + t\right). \tag{3}$$

Throughout this paper, we use $p(.)$ to represent the ideal projection, $p^b(.)$ for the detector blurred projection, $f(.)$ for the object function, and $h(.)$ for the detector response function (also referred as point spread function or PSF, which is frequently addressed in this paper). We also define $P(.)$, $F(.)$, and $H(.)$ to be their corresponding one–dimensional (1-D) or two-dimensional (2-D) Fourier transforms (FT) on their corresponding context.

B. Geometric Transfer Function for VFF Collimators

It has been shown by Zeng *et al.* that the defined CCS has the advantage that the GTFs for parallel-, fan-, and cone-beam geometries have the shift invariant property [18]. In this work, we employ the same geometric model in Fig. 2 to study the PSF properties of VFF geometry. Following the derivations of Metz *et al.* and Tsui *et al.* [19], [20], one can obtain the GTF for VFF geometry in terms of the integral of the aperture function (using the similar definition and notation, as in [19] and [20])

$$\phi_{\mathrm{VFF}}(\mathbf{r_0}, \mathbf{r}) = \mathbf{K} \iint a(-\sigma)a(\mathbf{r}_T - \sigma)d^2\sigma \tag{4}$$

where

$$\mathbf{K} = \frac{Z + L + B}{4\pi A\left[(Z + L + B)^2 + (x - x_0)^2 + (y - y_0)^2\right]^{3/2}} \tag{5}$$

and

$$r_{Tx} = \frac{L}{Z + L + B}(x - x_0) \tag{6}$$

$$r_{Ty} = \frac{L}{Z + L + B}\left[\frac{D - Z}{D + L}y - \frac{D + L + B}{D + L}y_0\right] \tag{7}$$

where the focal length D in (7) is a function of y, i.e., $D = D(y)$.

Note that (4) becomes the GTF for fan-beam geometry if the focal length D is a constant. For this geometry, when the above CCS is applied, we have

$$(x_0, y_0) = \left(x_{0C}, y_{0C} = \frac{D + L + B}{D - Z}y_0\right) \tag{8}$$

hence

$$r_{Ty} = \frac{L}{Z + L + B}\left[\frac{D - Z}{D + L}(y - y_{0C})\right]. \tag{9}$$

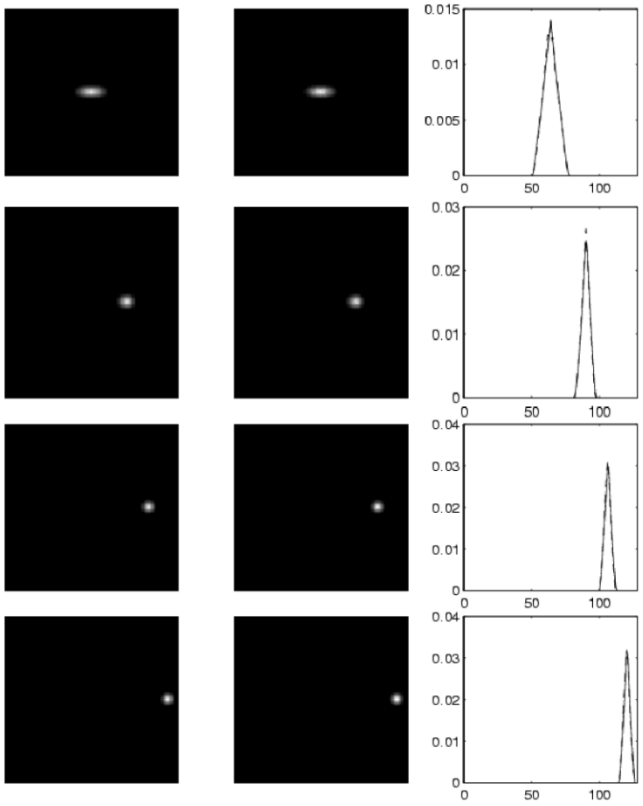

Fig. 3. Comparison of calculated geometrical PSF (left column) with Monte Carlo simulation (middle column) at depth 35 cm and offset of 0, 5, 10, and 15 cm, respectively (from top to bottom). The right column shows the profiles through the center of the geometric PSF, with the theoretical calculation in the solid line and the Monte Carlo simulation in the dashed line (1 pixel = 0.3438 cm).

Therefore, the GTF for parallel- or fan-beam can be expressed as

$$\phi_{Fan}(\mathbf{r}_{0C}, \mathbf{r}) = \phi(x - x_{0C}, y - y_{0C}, z) \tag{10}$$

which reflects the *shift invariant* property of parallel- or fan-beam collimator at any plane with a fixed distance z to the collimator surface. However, for VFF geometry, this shift invariant property no longer holds. Using the same CCS, the GTF of VFF collimator can only be written as

$$\phi_{\text{VFF}} = \phi(x - x_{0C}, y, y_{0C}, z). \tag{11}$$

In Fig. 3, we compared the Monte Carlo simulation results with our calculated geometric PSFs for VFF collimators. The focal-length function is $D(\xi) = a + b|\xi|$ with $a = 150$ pixel units, $b = 2.5$. The shift variance is clearly observed in the plots.

III. Method

A. FDR and its Limitation in Nonparallel Geometries

The 2-D FT $P(n, \omega)$ of a sinogram of projection data $p(\theta, \xi)$ is given by

$$P(n, \omega) = \int_0^{2\pi} d\theta \int_{-\infty}^{\infty} d\xi e^{-i(n\theta + \omega\xi)} p(\theta, \xi) \tag{12}$$

where n and ω are the angular frequency (corresponding to the projection angle θ) and spatial frequency (corresponding to the position on the detector ξ), respectively. The complex exponential in the integrand of (12) can be interpreted as a 2-D plane wave in the n-ω plane [10], and its phase $n\theta + \omega\xi$ and amplitude $p(\theta, \xi)$ depend on θ and ξ. The plane wave is a fast oscillating function of θ and ξ, so the integration of (12) is approximately zero except for $n\theta + \omega\xi = c + 2k\pi$, where c is a constant and k is an integer. Taking the derivative with respect to θ on both sides, as n and ω do not depend on θ, we have

$$\frac{d\xi}{d\theta} = -\frac{n}{\omega}. \tag{13}$$

For parallel geometry, recall the relationships (1)–(3) in CCS; we have the following FDR:

$$P(n, \omega) \neq 0 \text{ for } \eta = -\frac{n}{\omega} + R = \eta(n, \omega). \tag{14}$$

Note that (13) originally derived from the parallel-beam geometry is still true for other geometries. By applying (1)–(3) to a VFF collimation, we have

$$\frac{d\xi}{d\theta} = \frac{D^2(\eta - R) - \xi^2(D - \eta)}{D(D - \eta) + \xi\eta D'} \tag{15}$$

where D' denotes the derivative of the focal length function $D(\xi)$ with respect to ξ for VFF geometry and becomes 0 for a fan-beam geometry. The FDR is then obtained using (13) and (15) as

$$P(n, \omega) \neq 0 \text{ for } \frac{n}{\omega} = \frac{\xi^2(D - \eta) - D^2(\eta - R)}{D(D - \eta) + \xi\eta D'} \tag{16}$$

or rewritten as

$$\eta = \frac{nD^2 - \omega D(DR + \xi^2)}{n(D - D'\xi) - \omega(D^2 + \xi^2)} = \eta(n, \omega, \xi). \tag{17}$$

For a fan-beam geometry, (17) is simplified as

$$\eta = \frac{nD^2 - D\omega(DR + \xi^2)}{nD - \omega(D^2 + \xi^2)} = \eta(n, \omega, \xi) \tag{18}$$

and when $D \to \infty$, it degenerates to the parallel FDR (14).

To apply the filtering techniques to the compensation of the spatially variant PSF blurring effect, it requires: 1) that the blurred projection data can be written as a convolution of the object with the PSF with respect to the spatial variable ξ and 2) that FDR can be applied to carry out the dependency of the detector response on the other spatial variable η. For example, with parallel-hole collimation, a blurred projection can be expressed as

$$p^b(\theta, \xi) = \int_{-\infty}^{\infty} d\xi' \int_{-\infty}^{\infty} d\eta' f^{\theta}(\xi', \eta') h(\xi - \xi', \eta') \tag{19}$$

then its 2-D FT with FDR applied can be expressed as

$$P^b(n, \omega) \approx \int_0^{2\pi} d\theta e^{-in\theta} \int_{-\infty}^{\infty} d\xi' e^{-i\omega\xi'} f^{\theta}(\xi', \eta(n, \omega)) \times H\left(\omega, \frac{-n}{\omega} + R\right). \tag{20}$$

The two integrals together in (20) is a 2-D FT of ideal projection, therefore the compensation can be done using the following equation, where a filtering technique is applicable:

$$P(n,\omega) = P^b(n,\omega)H^{-1}\left(\omega, \frac{-n}{\omega} + R\right) \tag{21}$$

(for more details, see [6]–[8]).

However, as shown in Section II, for VFF geometry, the blurred projection is no longer a convolution and has the form

$$p^b(\theta,\xi) = \int_{-\infty}^{\infty} d\xi' \int_{-\infty}^{\infty} d\eta' f^\theta(\xi',\eta')h(\xi,\xi',\eta') \tag{22}$$

and the FDR (17) above still involves spatial variable ξ, therefore both conditions 1) and 2) above are not satisfied. These obstacles make it impossible to formulate a relation like (21) without approximations. In general, for parallel beam geometry, one can find a pure frequency-domain filter with

$$P_{\text{ideal}}(n,\omega) = P_{\text{blur}}(n,\omega)H^{-1}(n,\omega)$$

but for nonparallel geometries, we encounter the following integral in general:

$$P_{\text{ideal}}(n,\xi) = \int ds P_{\text{blur}}(n,s)H^{-1}(n,\xi,s). \tag{23}$$

In general, the computation of an integral similar to (23) is not as efficient as the filtering technique. However, since it is a 1-D integration here, the computational cost will not be a limiting factor.

B. Kernel Matrix Multiplication

Equation (23) in discrete form is basically a vector P from the FT of the blurred projection data multiplied by a matrix H^{-1}. To find out H^{-1} in this equation, let us first consider the ideal projection (i.e., no detector blurring) $p(\theta,\xi)$ in the polar coordinate system, which is a line integral of the source distribution $f(\rho,\beta)$ along the corresponding projection ray l, as shown in Fig. 4

$$p(\theta,\xi) = \int_{-\infty}^{\infty} f^\theta(\rho,\beta)dl \tag{24}$$

where $f^\theta(\rho,\beta) = f(\rho,\varphi = \beta+\theta)$ is the object function expressed in the polar coordinate system rotated by θ degree, and the projection ray l is determined by $\rho\cos(\beta-\alpha) = q$ as shown in Fig. 4 or expressed as

$$l: \begin{cases} s = \rho\cos\beta = \frac{q\cos\beta}{\cos(\beta-\alpha)} \\ t = \rho\sin\beta = \frac{q\sin\beta}{\cos(\beta-\alpha)} \end{cases}. \tag{25}$$

Transform the line integral variable l into β, and we have

$$\begin{aligned} dl &= \sqrt{\left(\frac{ds}{d\beta}\right)^2 + \left(\frac{dt}{d\beta}\right)^2}d\beta \\ &= \left|\frac{q}{\cos^2(\beta-\alpha)}\right| d\beta \end{aligned} \tag{26}$$

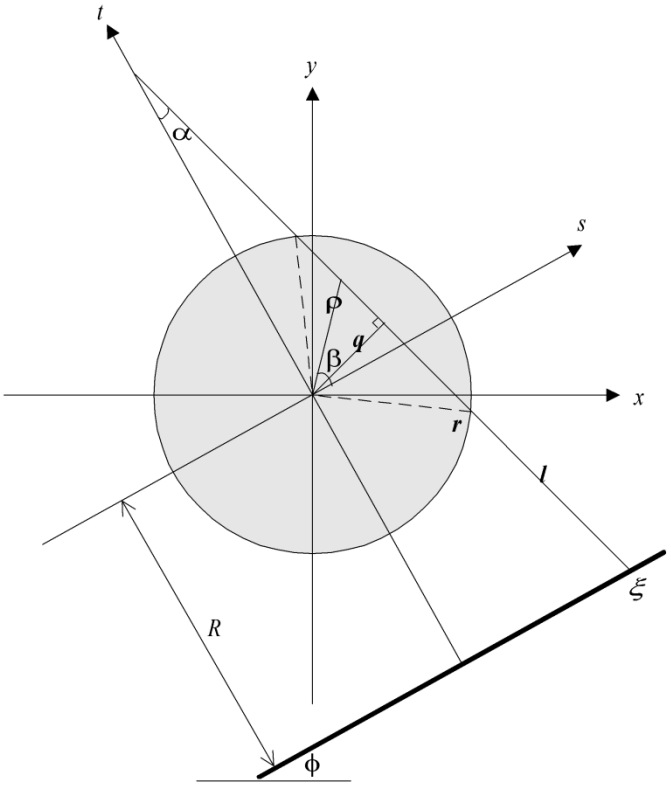

Fig. 4. Projection ray l in polar coordinate system: $\rho\cos(\beta-\alpha) = q(\xi)$, $\beta \in (\alpha-\gamma, \alpha+\gamma)$, where $\gamma = \cos^{-1}(q(\xi)/r)$ and r is the radius of the object support.

and

$$p(\theta,\xi) = \int_{\alpha-\pi/2}^{\alpha+\pi/2} f^\theta\left(\frac{q}{\cos(\beta-\alpha)},\beta\right)\left|\frac{q}{\cos^2(\beta-\alpha)}\right| d\beta. \tag{27}$$

Note that q and α are functions of ξ depending on the collimator geometry

$$\begin{aligned} \alpha(\xi) &= \tan^{-1}\left[\frac{\xi}{D(\xi)}\right] \\ q(\xi) &= [D(\xi) - R]\sin\alpha \end{aligned} \tag{28}$$

where $D(\xi)$ is the focal-length function and R is the radius of rotation.

If the object has a finite compact support with radius r, by defining

$$\begin{aligned} w(\xi,\theta) &\equiv \left|\frac{q(\xi)}{\cos^2\theta}\right| \\ \gamma &\equiv \cos^{-1}\left[\frac{q(\xi)}{r}\right] \end{aligned} \tag{29}$$

we can write the ideal projection (27) as

$$\begin{aligned} p(\theta,\xi) &= \int_{\alpha-\gamma}^{\alpha+\gamma} f\left(\frac{q(\xi)}{\cos(\beta-\alpha)},\beta+\theta\right)w(\xi,\beta-\alpha)d\beta \\ &= \int_{-\gamma}^{\gamma} f\left(\frac{q(\xi)}{\cos(\beta)},\beta+\theta+\alpha\right)w(\xi,\beta)d\beta. \end{aligned} \tag{30}$$

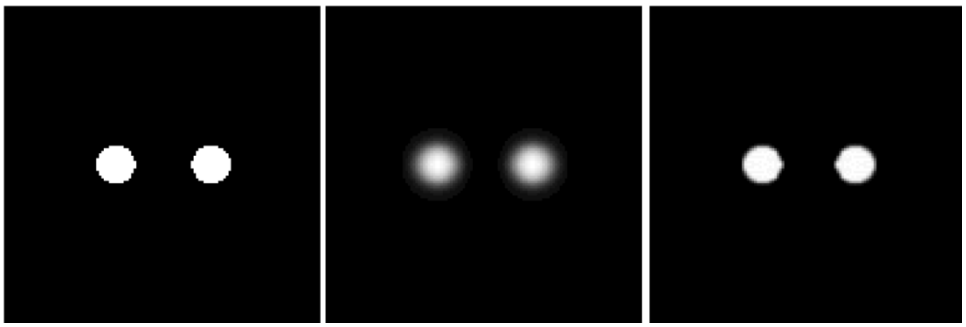

Fig. 5. Fan-beam collimated SPECT studies on reconstructed images, where the focal length $D = 200$ pixel units. From left to right are the original phantom, the reconstruction image without detector response compensation, and the reconstructed image with compensation using kernel matrix method, respectively.

Its FT with respect to variables θ is given by

$$P(n,\xi) = \int_{-\gamma}^{\gamma} F\left(\frac{q(\xi)}{\cos(\beta)}, n\right) w(\xi,\beta) e^{in\beta + in\alpha} d\beta$$
$$= e^{in\alpha} \int_{-\gamma}^{\gamma} F\left(\frac{q(\xi)}{\cos\beta}, n\right) w(\xi,\beta) e^{in\beta} d\beta \quad (31)$$

where $F(.)$ is the FT, more precisely, the Fourier series expansion of $f(.)$.

On the other hand, a general detector blurred projection can be expressed in the polar coordinate system as the following 2-D integral:

$$p^b(\theta, s) = \int_{R^2} f(\rho,\varphi) h(\rho,\varphi;\theta,s) \rho d\rho d\varphi \quad (32)$$

where $h(\rho,\varphi;\theta,s)$ is the system point response [corresponding to each point (ρ,φ)], which can be measured during the system calibration process. Note that $h(.)$ only depends on the relative position of the source point to the detector bin. Therefore, it is actually determined by ρ, s, and $\varphi - \theta$. By defining

$$g(\rho, s; \theta - \varphi) \equiv h(\rho,\varphi;\theta,s)\rho \quad (33)$$

we have

$$p^b(\theta, s) = \int_{R^2} f(\rho,\varphi) g(\rho, s; \theta - \varphi) d\rho d\varphi. \quad (34)$$

The 1-D FT on (34) with respect to θ gives the following linear equation:

$$P^b(n, s) = \int_0^{\infty} F(\rho, n) G(\rho, s; n) d\rho \quad (35)$$

where $G(.)$ is similarly defined as the FT of $g(.)$, and we can estimate $F(.)$ by

$$\hat{F}(\rho, n) = \int_{-\infty}^{\infty} P^b(n, s) G^{-1}(\rho, s; n) ds. \quad (36)$$

Substitute (36) into (31), and we have

$$\begin{aligned} &P(n,\xi) \\ &= e^{in\alpha} \\ &\times \int_{-\gamma}^{\gamma} \left\{ \int_{-\infty}^{\infty} P^b(n,s) G^{-1}\left(\frac{q(\xi)}{\cos\beta}, s; n\right) ds \right\} w(\xi,\beta) e^{in\beta} d\beta \\ &= \int ds P^b(n,s) \int d\beta e^{in\beta} w(\xi,\beta) G^{-1}\left(\frac{q(\xi)}{\cos\beta}, s; n\right) e^{in\alpha} \\ &= \int ds P^b(n,s) H^{-1}(\xi, s; n) \end{aligned} \quad (37)$$

where

$$H^{-1}(\xi, s; n)$$
$$= e^{in\alpha} \int_{-\gamma}^{\gamma} d\beta e^{in\beta} w(\xi,\beta) G^{-1}\left(\frac{q(\xi)}{\cos\beta}, s; n\right)$$
$$= e^{in\alpha} \int_{-\gamma}^{\gamma} d\beta e^{in\beta} G^{-1}\left(\frac{q(\xi)}{\cos\beta}, s; n\right) \left|\frac{q(\xi)}{\cos^2\beta}\right|. \quad (38)$$

The pseudoinverse of G in (36) can be performed by the singular value decomposition (SVD) method. It may take some time to construct the matrix H^{-1}, but once it is obtained, its use is a 1-D integral as indicated by (23), which can be efficiently computed.

Furthermore, this method presents a unified compensation framework for VFF, fan-, and parallel-beam geometries with the only difference in expressing the geometry functions $q(\xi)$ and $\alpha(\xi)$.

IV. Simulation Results

To validate the proposed kernel matrix method, we simulated blurred projection data using both fan-beam and VFF collimators with the GTF as the detector response function. For fan-beam, the focal length is 200 pixel units. For VFF, the focal length function is $a+b|\xi|$, with $a = 150$ pixel units and $b = 2.5$. The source phantoms are shown in Figs. 5 and 7. From each phantom, 128 noise-free projections were simulated evenly over 360° in a circular scan orbit. Each projection has 128 bins evenly distributed along the detection plane. The compensation was applied to the blurred projection data before image reconstruction, and the reconstruction was done analytically with the algorithm described in [17].

A. Fan-Beam Spheres Phantom Experiment

To show the resolution improvement by our new method, we first demonstrated a simple phantom with two small spheres, each has radius of 3 cm and separated by 6.875 cm as shown in the first picture in Fig. 5. The reconstruction from the blurred data and from our kernel matrix method correction data are presented for comparison in Fig. 5 as well. The kernel matrix method greatly improves the resolution in the reconstructed image that can be visually observed. In Fig. 6, we also plot the profiles along the central horizontal line of Fig. 5, which clearly shows the improvements.

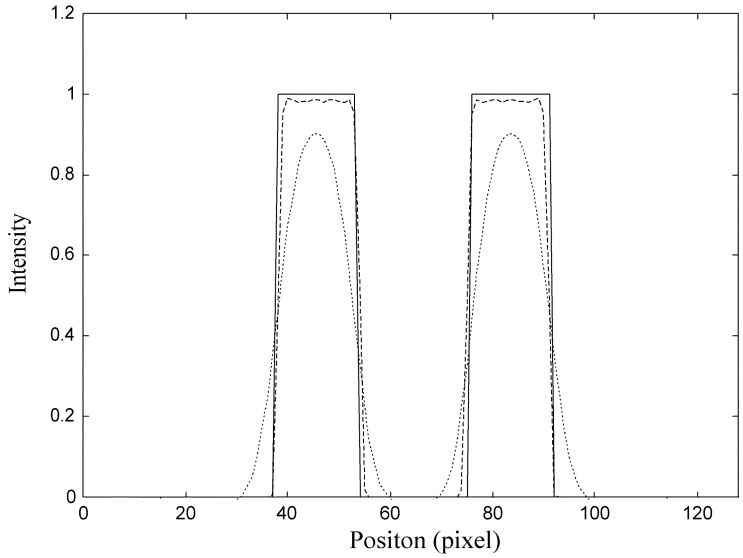

Fig. 6. Profiles of the images presented in Fig. 5 along the central horizontal line. The solid, dotted, and dashed lines represent profiles for the phantom, the reconstructed image without compensation, and the reconstructed image with compensation using kernel matrix method, respectively.

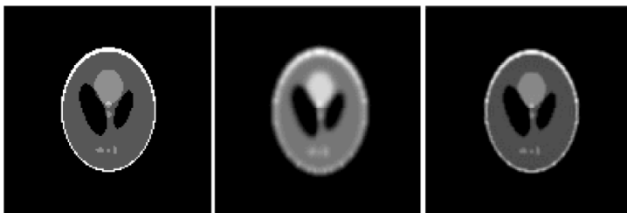

Fig. 7. VFF collimated SPECT studies on reconstructed images, where $D(\xi) = a + b|\xi|$, $a = 150$ pixel units, and $b = 2.5$. From left to right are the Shepp–Logan phantom, the reconstructed image without compensation, and the reconstructed image with compensation using kernel matrix method.

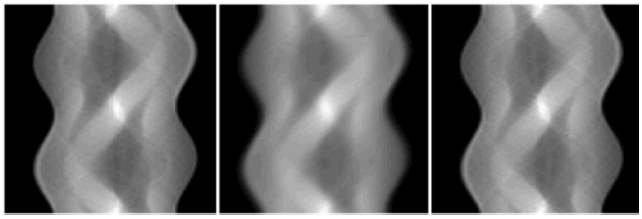

Fig. 8. VFF collimated SPECT studies on sinograms, where $D(\xi) = a + b|\xi|$, $a = 150$ pixel units, and $b = 2.5$. From left to right are the ideal sinogram from the Shepp–Logan phantom, the simulated collimator blurred sinogram, and the corrected sinogram using our kernel matrix method.

B. VFF-Beam Shepp–Logan Phantom Experiment

In this experiment, we applied our method to the VFF geometry with a more complicated phantom, the Shepp–Logan phantom. The results are compared in both sinogram space and image space, where a better image quality can be found after correction using the kernel matrix method as shown in Figs. 7 and 8.

From these results we observed that the proposed kernel matrix method achieves accurate compensation in terms of image resolution.

V. Discussion and Conclusion

In conclusion, we proposed a new kernel matrix method for accurate detector blurring correction in SPECT with nonparallel geometries.

First, the GTF and FDR were studied for fan-beam and VFF geometries following the scheme used in parallel beam SPECT. Based on these studies, the limitation of FDR-filtering strategy was clearly observed, and a kernel matrix multiplication method was then presented, which can eliminate the approximation in conventional filtering techniques and has demonstrated improved performance.

We tested the proposed method by digital phantoms using fan-beam and VFF collimators. The proposed kernel matrix method employs a fully calibrated system imaging kernel matrix and shows accurate compensation for the spatially variant detector response, as expected. Although noiseless simulations were performed in this paper, the results indicate that the method has the potential for deblurring projection data and hence for improving the fidelity of the reconstructed images.

References

[1] A. R. Formiconi, A. Pupi, and A. Passeri, "Compensation of spatial system response in SPECT with conjugate gradient reconstruction technique," *Phys. Med. Biol.*, vol. 34, pp. 69–84, 1990.

[2] B. M. W. Tsui, H. B. Hu, D. R. Gilland, and G. T. Gullberg, "Implementation of simultaneous attenuation and detector response correction in SPECT," *IEEE Trans. Nucl. Sci.*, vol. 35, pp. 778–783, 1988.

[3] G. L. Zeng, G. T. Gullberg, B. M. W. Tsui, and J. A. Terry, "Three-dimensional iterative reconstruction algorithm with attenuation and geometric point response correction," *IEEE Trans. Nucl. Sci.*, vol. 38, pp. 693–702, 1991.

[4] Z. Liang, T. G. Turkington, D. R. Gilland, R. J. Jaszczak, and R. E. Coleman, "Simultaneous compensation for attenuation, scatter, and detector response of SPECT reconstruction in three dimensions," *Phys. Med. Biol.*, vol. 37, pp. 587–603, 1992.

[5] G. Han, "Image reconstruction in quantitative cardiac SPECT with varying focal-length fan-beam collimators," Ph.D. dissertation, State Univ. New York, Stony Brook, NY, 2000.

[6] P. R. Edholm, R. M. Lewitt, and B. Lindholm, "Novel properties of the fourier decomposition of the sinogram," in *Proc. SPIE Int. Workshop Physics Eng. Computerized Multidimensional Image Processing*, 1986, pp. 169–173.
[7] R. M. Lewitt, P. R. Edholm, and W. Xia, "Fourier method for correction of depth-dependent blurring," *SPIE Med. Imaging III*, vol. 1092, pp. 232–239, 1989.
[8] S. J. Glick, B. C. Penney, M. A. King, and C. L. Byrne, "Noniterative compensation for the distance-dependent detector response and photon attenuation in SPECT imaging," *IEEE Trans. Med. Imaging*, vol. 13, pp. 363–374, 1994.
[9] W. G. Hawkins, P. K. Leichner, and N. Yang, "The circular harmonic transform for SPECT reconstruction and boundary conditions on the fourier transform of the sinogram," *IEEE Trans. Med.Imaging*, vol. 7, pp. 135–148, 1988.
[10] W. Xia, R. M. Lewitt, and P. R. Edholm, "Fourier correction for spatially variant collimator blurring in SPECT," *IEEE Trans. Med. Imaging*, vol. 14, pp. 100–115, 1995.
[11] J. Ye and Z. Liang, "Depth-dependent resolution deconvolution for myocardial perfusion SPECT with noncircular scan orbit," *J. Nucl. Medicine*, vol. 35, p. 190, 1994.
[12] Z. Cao and B. M. W. Tsui, "A filtering technique to compensate for detector response in converging-beam SPECT reconstruction," *Phys. Med. Biol.*, vol. 39, pp. 1281–1293, 1994.
[13] R. Novikov, "An inversion formula for the attenuated X-ray transformation," *preprint*, May 2000.
[14] L. Kunyansky, "A new SPECT reconstruction algorithm based on the Novikov's explicit inversion formula," *Inverse Problems*, vol. 17, pp. 293–306, 2001.
[15] H. Lu, J. Wen, X. Li, T. Li, G. Han, and Z. Liang, "Toward an analytical solution for 3D SPECT reconstruction with nonuniform attenuation and distance-dependent resolution variation: A Monte Carlo simulation study," *SPIE Med. Imaging*, vol. 4684, pp. 20–28, 2002.
[16] J. Wen, T. Li, X. Li, and Z. Liang, "Fan-beam and variable focal-length fan-beam SPECT reconstruction with nonuniform attenuation," *J. Nucl. Medicine Technol.*, vol. 30, p. 97, 2002.
[17] J. Wen, T. Li, and Z. Liang, "Ray-driven analytical fan-beam SPECT reconstruction with nonuniform attenuation," *Proc. IEEE Int. Symp. Biomedical Imaging*, pp. 629–632, 2002.
[18] G. L. Zeng and G. T. Gullberg, "Frequency domain implementation of the three-dimensional geometric point response correction in SPECT imaging," *IEEE Trans. Nucl. Sci.*, vol. 39, pp. 1444–1453, 1992.
[19] C. E. Metz, F. B. Atkins, and B. N. Beck, "The geometric transfer function component for scintillation camera collimators with straight parallel holes," *Phys. Med. Biol.*, vol. 25, pp. 1059–1070, 1980.
[20] B. M. W. Tsui and G. T. Gullberg, "The geometric transfer function for cone and fan beam collimators," *Phys. Med. Biol.*, vol. 35, pp. 81–93, 1990.